Interplay of phase-sensitive amplification and cascaded four-wave mixing in dispersion-controlled waveguides

Aude Martin,[1,2] Sylvain Combrié,[2] Amnon Willinger,[3] Gadi Eisenstein,[3] and Alfredo de Rossi[2,*]

[1]*Centre de Nanosciences et de Nanotechnologies, CNRS, Univ. Paris-Sud, Université Paris-Saclay, C2N Marcoussis, Marcoussis, 91460, France*

[2]*Thales Research and Technology, Palaiseau, 91120, France*

[3]*Technion Institute of Technology, Haifa, 3200003, Israel*

(Received 18 March 2016; published 5 August 2016)

Phase-sensitive parametric interactions can selectively process the two complex quadratures of the optical field. We implement phase-sensitive amplification in a large band-gap semiconductor photonic crystal waveguide in order to avoid two-photon absorption and free-carrier-related effects. Experimentally, an extinction ratio of 15 dB is achieved in a 1.5-mm-long photonic crystal waveguide, at a peak pump power of about 600 mW. We show that cascaded parametric interaction has a strong impact on squeezing and phase-sensitive extinction ratio and that this depends on the dispersion profile of the waveguide.

DOI: 10.1103/PhysRevA.94.023817

I. INTRODUCTION

Four-wave mixing (FWM) is a nonlinear optical parametric process which is ubiquitous in optical signal processing [1]. The opportunity to implement FWM in compact integrated photonic circuits has appeared with passive semiconductor waveguides, also owing to the very strong optical confinement, namely, in GaAs ring resonators [2] and silicon waveguides [3,4]. Here, the nonlinear coupling coefficient is very large, namely, $\gamma > 100\ \mathrm{m^{-1}\,W^{-1}}$, which is about 4 orders of magnitude larger than in highly nonlinear fibers.

A radically different approach exploits the confinement properties of photonic crystal (PhC) waveguides, where the group velocity can be decreased with moderate insertion losses to about $c/40$ [5]. Thus, on top of spatial confinement, low group velocity further enhances the nonlinear interaction. A very large nonlinear coupling ($\gamma > 6000\ \mathrm{m^{-1}\,W^{-1}}$) has been demonstrated in such waveguides [6].

The coherent nature of FWM implies that the interaction is maximized when the mutual phase is preserved along the propagation. This phase-matching condition is fulfilled by tailoring the dispersion, e.g., using dispersion-flattened optical fibers [7]. These PhC waveguides can be designed to provide a flattened dispersion over most of their transmission bandwidth [5] and, therefore, can be used for efficient FWM.

Another interesting situation is when the dispersion is shaped such that phase matching occurs when the interacting waves are set at prescribed wavelengths. This results into a narrowband parametric amplification, which can be used to control the propagation delay all optically [8]. Narrowband FWM has been demonstrated in PhC waveguides owing to dispersion engineering [9].

A more complicated case is when dispersion affects a parametric process indirectly, namely, by controlling *ancillary* parametric interactions taking place simultaneously. This is the case when phase-sensitive amplification (PSA) is perturbed by competing FWM processes. PSA is a parametric process where FWM provides a parametric gain which depends on the relative phase of the interacting waves. When a mode S is combined with a strong pump P, an idler I is generated and S is amplified, if P is strong enough [Fig. 1(a)]. If and additional mode S is input at the place of the idler, then amplification depends on the mutual phase of these inputs [Fig. 1(b)]. Thus, the relative phase governs the exchange of energy between the pump and the other modes. PSA leads to amplification without additive noise [10–12]. Depending on the implementation, one or both quadratures of the coherent signal are amplified with an ideal $F = 1$ noise figure of merit [13].

If other FWM processes are allowed to compete with PSA, then the exchange energy is modified, which affects the phase-sensitive gain. A common situation is when two strong pumps $\omega_{1,2}$ generate two idlers at $2\omega_1 - \omega_2$ and $2\omega_2 - \omega_1$. This has been analyzed in the context of optical fibers [14]. It is shown in Ref. [15] that the minimum gain $G_{\min}$ is lowered by these additional interactions, which leads to an increased phase-sensitive extinction ratio ($R_E = G_{\max}/G_{\min}$).

In general, the deamplification of the off-phase quadrature of the signal is an essential feature of PSA implying that both quantum fluctuations and classical noise can be reduced [16]. This enables the regeneration of phase-encoded signals [17,18], which has been demonstrated recently [19]. Interestingly, deamplification has been used to enhance the sensitivity in position detection [20].

In this paper, we investigate PSA in photonic crystal waveguides, which has been first reported in silicon devices [21]. It has been shown that free carriers generated by nonlinear absorption impact PSA, reducing the R_E [22]. Here, a large electronic band-gap (1.9 eV) semiconductor (GaInP) is used, which greatly reduces nonlinear absorption (Sec. III). This allows the study of a PSA process uniquely governed by dispersion and competing FWM interactions. The measurement is carried out with a scheme which is a combination of asynchronous sampling and heterodyne detection (Sec. II).

Thus, we consider here the situation where PSA is perturbed by additional FWM processes, where the signal S itself interacts with each of the pumps to generate idler modes [Fig. 1(d)]. We show that this leads to an increased extinction ratio of the PSA gain, which no longer follows a sinusoidal dependence on the phase of the inputs (Sec. V). The main point is that

*alfredo.derossi@thalesgroup.com

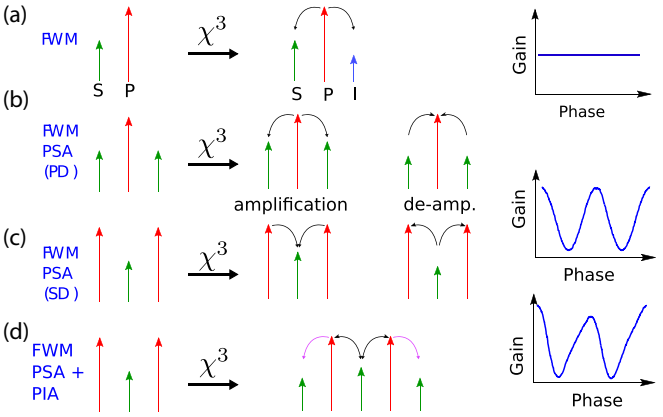

FIG. 1. Possible interactions involving four-wave mixing. (a) When the input idler is missing, parametric amplification does not depend on the mutual phase relationship between input waves and flow of energy (arrows) goes to the idler and the signal; (b) pump degenerate (PD) configuration with two signals, depending on the mutual phase, flow of energy goes from pump to signal or the other way round and amplification is phase-sensitive (PSA); (c) phase-sensitive process in the signal degenerate (SD) configuration; (d) competing FWM interactions (phase-insensitive) FWM may disturb the PSA process, resulting into a nonsinusoidal dependence on the phase.

the ancillary FWM processes can be controlled *independently* from the PSA by choosing a suitable dispersion. Depending on the phase matching of each of these processes, the amplification and deamplification are enhanced or depressed, relative to pure, phase-matched PSA (Sec. VI). Finally, in Sec. VII we show that the pump-degenerate configuration also reveals a strong dependence on auxiliary FWM interaction.

II. HETERODYNE MEASUREMENT OF THE PSA

The PSA is measured by injecting phase-locked inputs, obtained by a broad-band coherent source which is spectrally sliced, rephased, and finally amplified with an Erbium Doped Fiber Amplifier (EDFA). In order to avoid a phase-sensitive response in the EDFA, the pump and the signal are separated in time which, however, requires further retiming. This is done in Ref. [21] by using two wave shapers (Finisar). The output spectra are recorded as a function of the relative phase, which implies a tight control of the phase during the acquisition time of the optical spectrum analyzer (OSA).

Here, we introduce a different approach, where, instead, we use standard and low-cost telecom modules: two acousto-optics modulators (AOM), a telecom arrayed waveguide grating (AWG), and an optical band-pass filter (BPF) (Fig. 2). The source is a passively mode-locked (ML) femtosecond fiber laser (Optisiv) which, after a first stage filtering and amplifying, generates a 6-nm spectrally wide pulse which is then split in three different channels (labeled *a, b, c*, with $\lambda_a > \lambda_b > \lambda_c$) by the AWG. The corresponding autocorrelator traces reveal pulses with almost Gaussian profile and duration close to 9.5 ps (FWHM). Two of these channels (*a, c*) go through two delay lines and acquire a delay $\tau_{a,c}$, then they are recombined and go through AOM 1, while channel *b* goes through AOM 2,

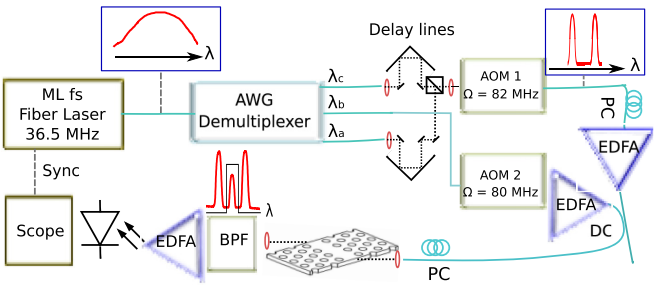

FIG. 2. Experimental setup for the measurement of the PSA. The ML fiber laser is spectrally sliced with an AWG demultiplexer. The three channels are synchronized and a relative frequency shift is applied using acousto-optic modulators. After combining, and polarization control, the signal is input to the PhC waveguide using microscope objectives. A band-pass filter is used to extract the signal before final amplification and detection.

so that *a, c*, on one side, and *b*, on the other, acquire the phases $\varphi_{1,2}(t) = -\Omega_{1,2}t$, respectively. Two EDFAs 1 and 2 are used to amplify channels *a, c* and channel *b* separately, which prevents PSA in the EDFA. The three channels are recombined after their polarization is independently adjusted to couple to the TE mode of the PhC waveguide.

In the one-mode configuration, the EDFAs are adjusted so that channels *a, c* are between 10 and 20 dB above

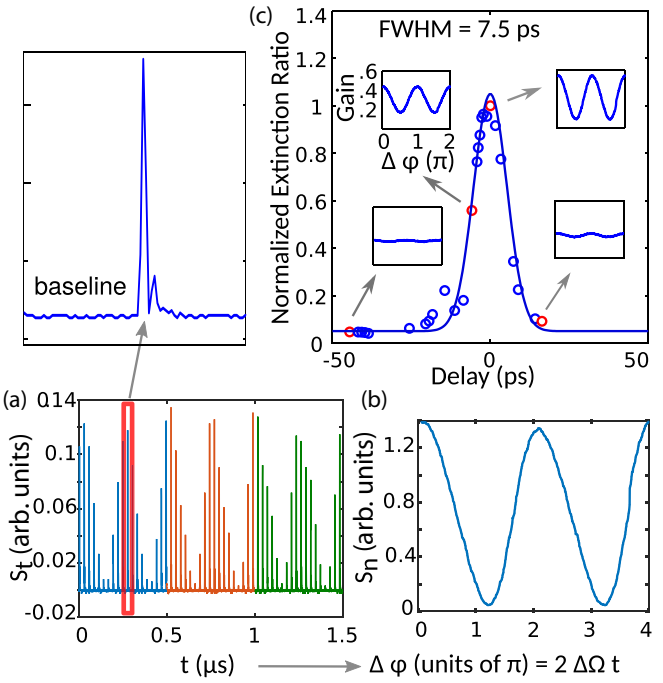

FIG. 3. PSA measurement. Oscilloscope trace (a) and magnified view of the pulse. The sample s_n is obtained after integration of the pulse s_t centered at time t. Then, samples are plotted in panel (b) after applying the mapping $\Delta\varphi = 2\Delta\Omega t$ in the interval $[0,4\pi]$. Color code in (a) represents adjacent periods mapped in the same interval to produce the highly resolved plot in (b). The extinction ratio, normalized to its maximum, is represented as a function of the mutual pulse delay in (c) and representative gain vs phase plot are in the inset associated to the red circles.

channel b, which plays the role of the signal. According to the theory of PSA [23], after propagation in the nonlinear waveguide, the signal will be amplified (and deamplified) with a sinusoidal dependence on the mutual phase of the interacting waves, namely, $\Delta\varphi = 2\varphi_b - \varphi_a - \varphi_c = 2(\Omega_1 - \Omega_2)t + \varphi_0 = 2\Delta\Omega t + \varphi_0$. The signal ($b$) is filtered (Fig. 3), amplified using a low-noise EDFA, detected (1-GHz photodiode), and displayed at the oscilloscope, which is synchronized with the repetition rate of the ML laser (36.5 MHz). A 20-μs-long trace s_t is recorded, entailing a sequence of pulses whose height reveals a sinusoidal modulation (Fig. 3) with period 250 ns, corresponding to the expected PSA gain law, where the gain follows a sinusoidal dependence $g = 1 + (1 - R_E)/(1 + R_E)\sin(2\Delta\Omega t + \varphi_0)$ on the phase.

The sequence s_t is mapped from time to phase (see Appendix) through $\Delta\varphi = 2(\Omega_1 - \Omega_2)t$ and folded in the domain $[0,4\pi]$. This produces a fairly well-resolved curve $s(\Delta\varphi)$, as shown in Fig. 3. The relative accuracy (standard deviation) is estimated to about 1%. We point out that using the AOMs introduces a heterodyne detection, therefore, the phase noise due to slow fluctuations of the optical path is ruled out. The measurement technique could be regarded as asynchronous sampling. Figure 3 also shows the dependence on the relative delay of the interacting pulses, which is clearly related to the pulse duration.

III. PHOTONIC CRYSTAL WAVEGUIDE

The device is a 1.5-mm-long single line defect waveguide made of an air-suspended GaInP membrane. The 180-nm-thick slab is patterned with a triangular lattice (period $a = 471$ nm) of holes. The first row of holes is displaced antisymmetrically along the waveguide axis by T_x. This induces the coupling of the odd and even modes which strongly modifies the dispersion [24]. Choosing $T_x = 0.1a$ results into a flat-band dispersion. Other small changes (see Appendix) are used for fine tuning.

Optical coherent tomography (OCT) is used to extract the dispersion and to estimate the propagation losses, as reported in Ref. [25]. The group index is approximately constant and equal to $n_g \approx 15$ over a bandwidth of about 15 nm, as shown in Fig. 4. Importantly, the waveguide dispersion β_2 changes sign twice at the zero dispersion wavelengths ($W_{ZD} = 1552.3$ and 1561 nm) so that in-between the dispersion is small $|\beta_2| < 0.4$ ps^2/mm. Coupling losses were reduced significantly with a mode adapter [26]. The attenuation is estimated to α is >30 dB/cm in the flat-band region, except for two transmission dips at 1550 and 1558 nm (Fig. 4), which are related to strong backscattering due to regularly spaced dislocations of the PhC. This is a known issue with long (e.g., about 1 mm) PhC waveguides. The nonlinear coupling coefficient γ is calculated (see Appendix) to be about 2000 W^{-1} m^{-1}. We consider an effective length due to linear attenuation $\alpha \approx 30$ dB/cm in the waveguide with physical length L, namely, $L_{\text{eff}} = (1 - e^{-\alpha L})\alpha^{-1} = 1$ mm.

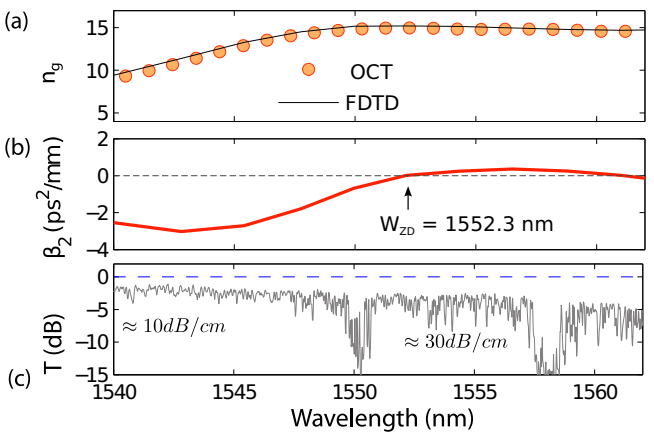

FIG. 4. OCT measurement and FDTD calculation of the waveguide dispersion. Group index (a), second-order dispersion (b), and transmission (c).

IV. COMPARISON WITH OTHER SEMICONDUCTOR DEVICES

In order to avoid the limitations due to nonlinear absorption, and, more importantly, the ensuing free-carrier dispersion and absorption, waveguides made of large band-gap materials ($E_g > 2\hbar\omega = 1.6$ eV at telecom wavelengths) have been developed. In particular, hydrogenated silicon [27], AlGaAs [28,29], GaInP [30], or chalcogenides waveguides [31].

Our device combines the large nonlinear coupling of PhC waveguides and the large nonlinear absorption threshold resulting from a large electronic gap. The large power density tolerated by the waveguide results net parametric gain (>10 dB), reached with about 0.6-W peak pump power [32].

In the configuration chosen for the PSA experiment, the maximum extinction ratio R_E achieved is 15 dB, at a maximum peak power of 0.6 W coupled in the device [see Sec. V and Fig. 6(c)]. Considering the link between the linearized conversion efficiency in FWM, $\eta = \gamma^2 L^2 P^2$, and the extinction ratio, this result is in line with expectations. This is apparent in Table I. Despite their low nonlinearity, low-loss waveguides with good nonlinear figure of merit such as chalcogenide [33] can reach high R_E by increasing pump power and device length. Conversely, the very large nonlinearity of silicon PhC offsets the larger propagation loss and also results in large R_E. Interestingly, the larger R_E in the GaInP PhC corresponds to a nearly identical linearized conversion efficiency η than in the silicon sample, which could be in part explained by the lack of free carriers. This point will be further discussed in Sec. VI. This is also consistent with the large $R_E = 20$ dB reported in long silicon waveguides, owing to a PN junction removing the free carriers generated

TABLE I. PSA in integrated waveguides.

γ (mm^{-1} W^{-1})	L (mm)	Power (W)	$\gamma^2L^2P^2$ dB	$G_{\max}$ dB	R_E dB	Ref.
0.01	65	6.7	13		18	[33]
4.3	0.2	2.3	5.9	3	11	[21]
0.28	40	0.22	8.2		20	[34]
2	1.5	0.65	5.8	3	15	This work

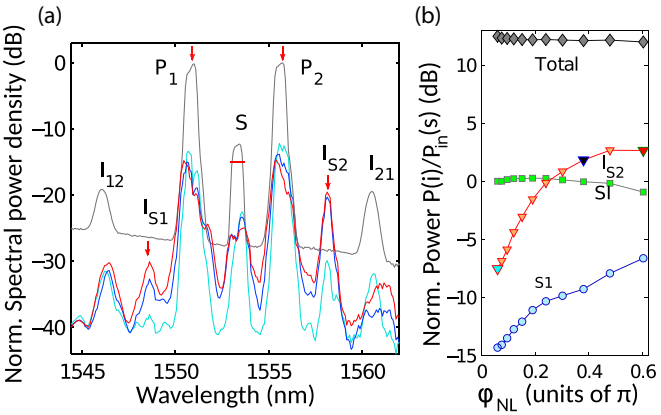

FIG. 5. One-mode PSA. (a) Spectral measurements: (gray) input signal normalized to 0 dB, with idlers I_{12} and I_{21} 18 dB below and ASE noise. Red arrows refer to the ITU grid. The red bar represents the spectral width of the ITU channel. Normalized output spectra (cyan, blue, and red) at different pump power (0.1, 0.6, and 0.9 W); integrated power in idler I_{S1}, I_{S2} and signal channels and total output (black), normalized by the input signal level, as a function of the nonlinear phase shift φ_{NL}. Color-coded symbols correspond to spectra in panel (a).

by nonlinear absorption [34]. Interestingly again, here η is only marginally larger than in the case of the silicon PhC.

V. SIGNAL DEGENERATE PSA

We first consider the signal degenerate [Fig. 1(c)] configuration. The PSA gain $g(\Delta\varphi)$ is measured (see Appendix) as a function of the input power. For clarity, we rather refer to the nonlinear phase shift $\varphi_{\mathrm{NL}} = \gamma P_P L_{\mathrm{eff}}$, which represents the nonlinear coupling, directly related to the (total) coupled peak input pump power P_P.

The input spectrum [Fig. 5(a)] consists of the dual pump (P_1, P_2), separated by 6 ITU dense wavelength domain multiplexing (DWDM) channels (i.e., 600 GHz) and the signal centered at 193 THz ($\lambda = 1553.3$ nm), the signal to (total) pump ratio is -12 dB. There is no BP filter after the EDFA, therefore, there are two idlers (I_{12} and I_{21}) generated in the amplifier, spectrally spaced by $\Delta\omega/2\pi = 600$ GHz each from the closest pump. Their level is 19 dB below the pump, and because of the waveguide dispersion the parametric interactions with the pumps or the probe are inefficient, we assume that they do not influence any of the results reported here.

In semiconductor waveguides, specifically silicon at telecom wavelengths, free-carrier effects are important, as mentioned above. The asymmetric spectral broadening of pulses is a signature of free-carrier dispersion (FCD). The symmetric pulse broadening observed here [Fig. 5(a)] indicates that FCD is negligible even when the nonlinear phase shift reaches a maximum of 0.6π, corresponding to about 1 W of total coupled peak pump power. Moreover, Fig. 5(b) shows that the total transmitted power remains proportional to the input (see Appendix) within the experimental error, therefore indicating negligible NL losses. The symmetry of the spectral broadening, which is therefore due to self- (SPM) and cross- (XPM) phase modulations, is preserved also because linear dispersion is negligible relative to the pulse bandwidth, as the characteristic lengths associated to second- and third-order dispersion are both at least 2 orders of magnitude larger than L.

TABLE II. Linear phase mismatch of FWM interactions.

$\lambda(S) - W_{ZD}$	$+1$ nm	$+0.15$ nm	-0.6 nm
$\Delta k(P_1,P_2,S)L_{\mathrm{eff}}$	$-0.15\,\pi$	$-0.07\,\pi$	$0.06\,\pi$
$\Delta k(P_1,S,I_{S1})L_{\mathrm{eff}}$	$0.33\,\pi$	$0.8\,\pi$	$1.2\,\pi$
$\Delta k(P_2,S,I_{S2})L_{\mathrm{eff}}$	$-0.4\,\pi$	$-0.3\,\pi$	$-0.2\,\pi$

The FWM process is governed by the phase mismatch $2\delta(P_1,P_2,S)L_{\mathrm{eff}} = \Delta k(P_1,P_2,S)L_{\mathrm{eff}} + \Phi_{\mathrm{NL}}$, entailing a linear and a nonlinear contribution [7,23]. In this configuration ($\lambda_s = W_{ZD} + 1$ nm), the linear contribution $\Delta k(P_1,P_2,S)L_{\mathrm{eff}} = (2k_S - k_{P_1} - k_{P_2})L_{\mathrm{eff}} \approx -\beta_2\Delta\omega^2$ is estimated to about -0.15π, implying the efficiency of the parametric interaction is close to the maximum also when Φ_{NL} increases.

Phase-sensitive interactions are not expected to show any specific signature in these spectral measurements since the integration time is much longer than the period of the phase modulation $1/\Delta\Omega$. What these measurements show, instead, is that strong FWM leads to the generation of two idlers I_{S1} and I_{S2}, due to the mixing of each pump with the signal. In Fig. 5(b), the relative power transferred to the two idlers is shown as a function of the pump power (i.e., the nonlinear phase shift). While the exact ratio may be overestimated while normalizing the spectra (see Appendix), it is apparent that the phase-insensitive FWM process I_{S2} is competing with the one-mode PSA. This is because the phase mismatch is small and negative, $\Delta k L_{\mathrm{eff}} = -0.4\pi$, therefore offset by Φ_{NL} as pump power is increased (Table II). The other idler is generated with much less efficiency because the phase mismatch is positive and is further increased by Φ_{NL}.

From theory [23], it is expected that the phase-sensitive gain $g(\Delta\varphi)$ should follow a perfectly sinusoidal dependence on the relative phase $\Delta\varphi$. Instead, experiment [Fig. 6(b)] shows that PSA $g(\Delta\varphi)$ is represented by a sinusoid only at moderate levels of nonlinearity ($\varphi_{\mathrm{NL}} < 0.2\pi$); then, the dependence becomes more complicated. Specifically, if we take the difference $\Delta\varphi(G_1,G_2) = \Delta\varphi|_{\max} - \Delta\varphi|_{\min}$ between $\Delta\varphi$ at maximum and minimum PSA, this decreases from π to about 0.7π [Fig. 6(a)], whereas theory predicts a strict π separation (sinusoidal dependence).

We note that a three-wave interaction, e.g., PSA, cannot explain this nonsinusoidal dependence. Other interactions must necessarily be involved, which is consistent with the spectral measurements [Fig. 5(b)].

We now consider the dependence of amplification $\{G_1 = \max[g(\Delta\varphi)]\}$ and deamplification $\{G_2 = \min[g(\Delta\varphi)]\}$ on the level of nonlinear coupling (φ_{NL}), which is shown in Fig. 6(c). While G_1 increases up to 2.3 dB, the deamplification (G_2) decreases much faster, so that the extinction ratio $R_E = G_1/G_2$ reaches 15 dB when $\varphi_{\mathrm{NL}} = 0.4$, with the total coupled peak power $P = 0.65$ W. Instead of being equal to 1, as in ideal PSA, the product $G_1 G_2 < 1$ and decreases as nonlinearity increases. Since nonlinear absorption here is small, we believe that in our case this nonideal response is mainly explained by

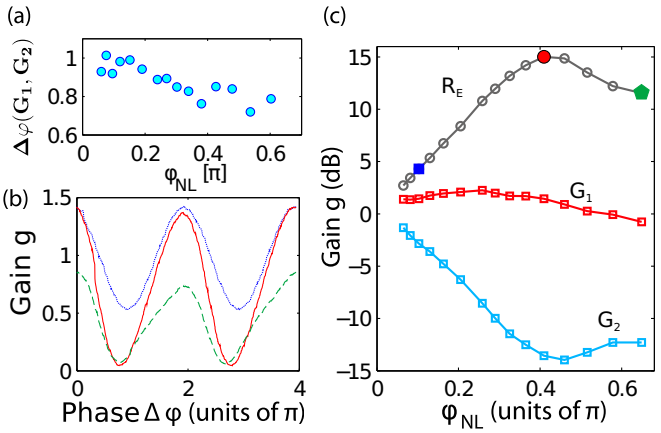

FIG. 6. Phase-sensitive gain g measurement on the signal S: (a) phase shift between minimum and maximum of g; (b) linear scale, as a function of the relative phase $\Delta\varphi$ and at different pump power level; (c) maximum and minimum gain $G_{1,2}$, and extinction ratio R_E, blue square (resp. red circle) corresponds to blue dotted line (resp. red line) in panel (b). The last point in panel (c) corresponds to the green dashed line in panel (b).

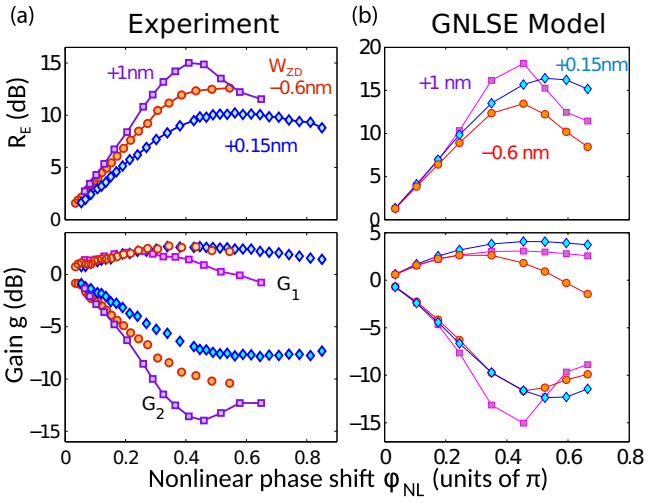

FIG. 7. Influence of the dispersion on the PSA dynamics. Measured (a) and calculated (b) extinction ratio R_E and phase-sensitive gain g as a function of the nonlinear phase shift φ_{NL}.

the strong self- and cross-phase modulations, broadening the signal spectra out of the window of the band-pass filter at the output. Modeling (see Sec. VI and Appendix) predicts G_1G_2 to be much closer to 1 as the pulse duration is increased by a factor 5 and to remain so as the NL coupling φ_{NL} increases.

The maximum of R_E is thus related to a minimum of G_2, which was indeed observed in optical fibers [15] and attributed to competing FWM interactions involving other waves. More generally, it was expected from theory that higher-order FWM harmonics may impact the phase-sensitive gain [14].

We believe this is indeed the case here. In particular, the idlers I_{S1} and I_{S2}, generated in the nonlinear waveguide, bear a dependence on the relative phase $\Delta\varphi$ at the input, therefore, they interact coherently with the signal S. Instead, idlers generated in the EDFA (I_{12} and I_{21}) are weak and they are not coupled to the signal by the strong pump, therefore, they do not influence the PSA process. All these measurements pinpoint the role of cascaded FWM in PSA, resulting into a large R_E.

In the next section, we discuss how this interaction results in drastically different dependence of the R_E on the injected power, when selecting different combinations of phase matching for each of them.

VI. ROLE OF THE WAVEGUIDE DISPERSION

In this section, we examine the situation where the PSA interaction is phase matched, thus supposedly maximized. Then, we repeat the measurement by varying the spectral position of the pump and the signal, still keeping the same spacing and relative power. This changes the phase-matching condition of the competing FWM interactions (S, P_1, I_{S1} and S, P_2, I_{S2}), while the PSA (S, P_1, P_2) remains phase matched ($|\Delta k L_{\mathrm{eff}}| \ll \pi$). This is detailed in Table II.

Self- and cross-phase modulations Φ_{NL} modify the phase matching. This contribution is positive and smaller than $\pi/2$, which slightly decreases the mismatch in interactions (P_1, P_2, S) and (P_2, I_{S2}, S) but increasing (P_2, I_{S1}, S). Thus, PSA remains phase matched, while one of the competing FWM processes is further mismatched.

When measuring the phase-sensitive gain [Fig. 7(a)], we observe that the peak of R_E is much less pronounced as the signal is placed at $+0.15$ nm or -0.6 nm from the W_{ZD}. Also, the slope of R_E versus the nonlinear coupling (φ_{NL}) decreases. It is apparent that R_E depends on the detuning (hence the dispersion and the mismatch of competing FWM) via G_2; specifically, the maximum of R_E is related to a minimum of G_2. Instead, G_1 has a weak dependence on the detuning, hence on competing FWM processes, with maximum ≈ 3 dB when $\lambda(S) = W_{ZD} + 0.15$ nm. The much stronger sensitivity of G_2 is because it results from a destructive interference, which is easily modified by any perturbation.

Thus, the phase-sensitive R_E dependence on the dispersion can be explained by competing FWM interactions. In order to further assess this point, we have modeled the PSA process using a generalized nonlinear Schrödinger equation (GNLSE), including the so-called all-orders dispersion. The model is detailed in the Appendix. We consider only the Kerr nonlinearity ($\chi^{(3)}$) and all the possible FWM interactions, and the exact dispersion of the waveguide (Fig. 4). We show that this is enough to reproduce the results as the detuning, hence, the phase matching of the processes involved, is changed. Then, we also add all possible corrections (free carriers, nonlinear absorption) and show that this is negligible. Thus, this identifies the dispersion as the sole possible explanation through the mechanism discussed above.

The calculated R_E [Fig. 7(b)] does show a peak which is particularly marked when $\lambda(S) = W_{ZD} + 1$ nm, namely, the same condition where the experiment reveals a peak. The maximum of R_E is less pronounced in the other configuration, as observed experimentally. The maximum gain reaches a value of 5 dB when the detuning from the W_{ZD} is 0.15 nm, still $G_1G_2 < 1$, as observed experimentally. More importantly, the minimum of G_2 is particularly marked, whereas it is much shallower as $\lambda(S)$ is changed. The calculated $g(\Delta\varphi)$ also

reproduces the nonsinusoidal behavior discussed above. Thus, the model reproduces the features observed experimentally, although there are some discrepancies hindering a very good quantitative agreement. Among the possible reasons, we believe that the uncertainty in the measured dispersion and the complicated spectral dependence of the waveguide losses might play a role. We also point out that we have not taken into account the nonlinear dispersion, which has recently been suggested to play an important role in photonic crystals [35].

We point out that a detailed analysis of how PSA is affected by competing FWM processes is extremely complex, particularly if dynamic effects (spectral broadening) are also to be considered. In the continuous wave (CW) regime and in fibers, this has been first considered in Ref. [15] and very recently analyzed in detail in Ref. [36]. What is shown here, instead, is that this complex dynamics is indeed controlled by the dispersion, and that the specific features observed, particularly the existence of a peak in the R_E, is robust to all the other effects, specifically, the inhomogeneous losses and spectral broadening.

This has practical implications as it means that very strong phase squeezing (deamplification) is possible in integrated photonic circuits owing to the contribution of higher-order FWM process, provided they are suitably controlled. This is indeed possible by exploiting dispersion engineering in PhC waveguides [5,24,37]. Achieving a large R_E is related to application to all-optical quantization of phase-encoded signals [38,39].

VII. PUMP-DEGENERATE PSA

The pump-degenerate PSA involves two signals. When one is the phase-conjugate replica of the other and the mutual phase is set suitably, both quadratures are amplified with a noise figure approaching 0 dB [13]. In this configuration pump harmonics are absent, however, there is still the possibility that pump and signal generate additional idlers, which could then compete with the PSA process. We note also that the phase mismatch has opposite sign relative to the signal degenerate case (i.e., when pump and signal are exchanged).

We have investigated this scenario by reconfiguring the input signal to consist in a pump wavelength centered at 1553.3 nm and the two signals are each 10 dB below the pump level. Since the two signals have the same phase (i.e., they are not conjugated in this configuration), the amplification still keeps the sinusoidal dependence on the relative phase.

We have performed the experiment on a nominally identical waveguide, with almost identical dispersion, but W_{ZD} located at 1553.6 nm. Here, the PSA interaction is virtually phase matched $[\Delta k(P_1,P_2,S)L_{\text{eff}} = -0.14\ \pi]$, as well as the FWM process generating an idler on the low-energy side $[\Delta k(P_2,S,I_{S2})L_{\text{eff}} = 0.4\ \pi]$. The other interaction is instead much less effective because of large phase mismatch $\Delta k(P_1,S,I_{S1})L_{\text{eff}} = -1.3\ \pi$. The output spectra in Fig. 8 clearly reveal the strong increase of I_{S2}, while I_{S1} is much less affected, consistently with the phase-matching condition. The PSA process is analyzed by filtering this time either S_1 or S_2. Interestingly, the phase-sensitive gain g differs substantially in the two cases, as apparent in Fig. 9(a). When observing S_1, the G_1 rises up to 6 dB, while when observing S_2, G_1 barely reaches 2 dB. Conversely, G_2 reaches a lower minimum when it is extracted from S_2. Also, the difference $\Delta\varphi$ between the maximum and minimum of g is close to π in the case of S_1, but decreases to 0.7π when S_2 is analyzed. This is interesting when considering that S_1 and S_2 belong to the same phase-sensitive FWM process. All this is consistent with the interpretation that the competing FWM processes have a strong influence in the PSA dynamics. Specifically, the interaction involving I_{S2} and S_2 is strong and therefore S_2 is strongly modified, which is not the case for S_1. The GNLSE model [Fig. 9(b)] reproduces well this behavior, namely, that $G_1(S_1) > G_1(S_2), G_2(S_1) > G_2(S_2)$. While G_1 appears to be in quantitative agreement for both S_1 and S_2, the minimum gain G_2 is expected to be much lower (stronger deamplification). We point out, however, that G_2 is more prone to error because it results from destructive interference.

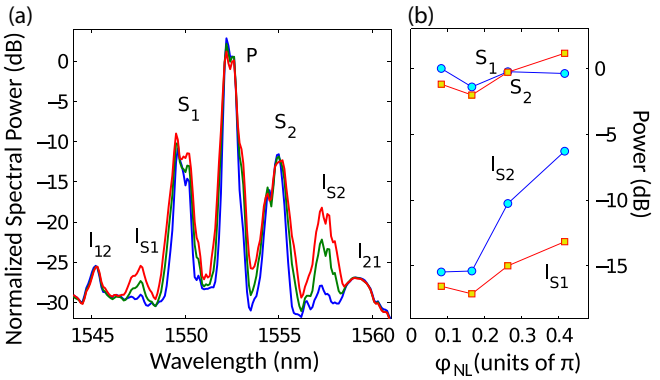

FIG. 8. Pump-degenerate PSA. Normalized output spectra at $\varphi_{\text{NL}} = 0.1\pi, 0.3\pi, 0.4\pi$, e.g., pumps 0.1, 0.3, and 0.6 W (a) and spectral power in the idlers and in the signal (b).

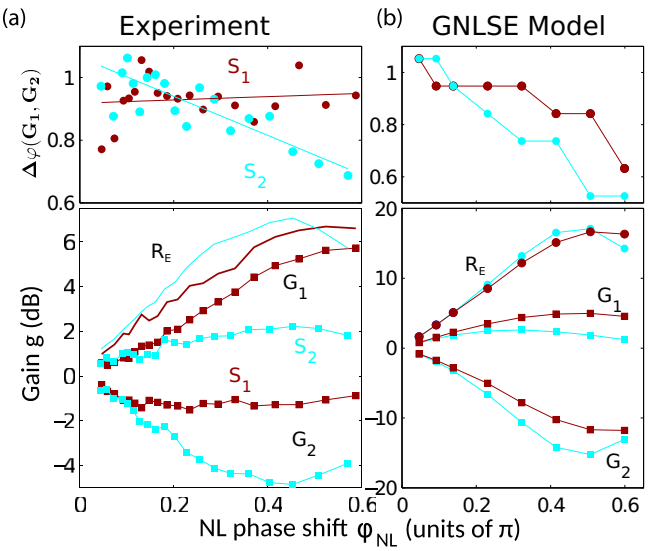

FIG. 9. Pump-degenerate PSA measured on S_1 (dark red or dark gray) or S_2 (cyan or light gray). The measured (a) and calculated (b) minimum G_2 and the maximum G_1 of the phase-sensitive gain g are plotted (bottom) along with their relative spacing (top) $\Delta\varphi$. The measured and calculated extinction ratio (R_E) is also plotted.

VIII. CONCLUSIONS

We have measured phase-sensitive amplification in a 1.5-mm-long GaInP photonic crystal waveguide using a heterodyne technique and asynchronous sampling. A maximum extinction ratio of 15 dB is reached at a coupled peak pump power of 650 mW. At larger power levels, we observe a nonsinusoidal dependence of PSA on the mutual phase which cannot be explained without accounting for the interference with competing FWM interactions. This also leads to the existence of a maximum of R_E, related to strong squeezing, as power is increased. We show that the interplay of the FWM interactions depends on the phase matching of each of those, which is ultimately related to the dispersion profile of the waveguide. We speculate that the phase-sensitive amplification could be optimized by a suitable shaping of the waveguide dispersion, which photonic crystal waveguides allow. Conversely, understanding these interactions might be important in avoiding unwanted distortion of the signal.

It is shown that the experimental results are very well reproduced by a time-domain model considering instantaneous Kerr nonlinear response and the very accurate description of the waveguide dispersion only and that other corrections are negligible. This is because of the use of a large-gap semiconductor alloy (GaInP), which minimizes nonlinear absorption and the ensuing generation of free carriers. Thus, this 1-mm-sized semiconductor waveguide effectively reproduces the properties of a nonlinear fiber, without however limitations such as Brillouin scattering. For some applications, the limited available bandwidth (10 to 20 nm) might be an acceptable price to pay.

Finally, we point out that experiment have been performed in the pulsed regime and, therefore, gain is limited by dynamical effects such as spectral broadening due to cross and self-phase modulation. A new generation of nonlinear waveguides with a solid cladding and optimized thermal conductivity would be able to sustain CW operations, and, therefore allow a practical implementation of phase-sensitive optical signal processing.

ACKNOWLEDGMENTS

We are indebted with F. Bretenaker, C. Husko, F. Raineri, and A. Mosk for valuable and enlightening comments. This work was supported by IDEX AAP IDI 2013 Grant No. 37-2013. We also acknowledge support by the European Research Council (ERC), project PHAROS (Grant No. 279248, P.I A. P. Mosk).

APPENDIX

1. Extraction of the phase-sensitive gain

First, an oscilloscope trace s_t is converted into a discrete series $s_n = \int_{t-\Delta t}^{t+\Delta t} s(t')dt'$ by integrating around the peak after having removed the background noise (the baseline). Then, the time axis is mapped as $t \to \Delta\varphi = 2\Delta\Omega t$ in the interval $[0,4\pi]$. The input power level is controlled by a variable attenuator just before coupling into the sample, therefore, the total pump power is $P = AP_{\max}$ and the pump to signal ratio is kept constant. A reference $s_0(\Delta\varphi)$ is taken with pump set to zero and it is normalized with the current attenuation A_0. Thus, the phase-sensitive gain is then estimated as $g(\Delta\varphi, A) = \frac{s(\Delta\varphi,A)A_0}{s_0(\Delta\varphi)A}$. We note that there is an unknown offset for the mutual phase $\Delta\varphi$, which is intrinsic to our heterodyne technique. Thus, we arbitrarily set the zero to the first maximum of g.

2. Normalization of the output spectra

Output spectra S_{OSA} are measured just at the output of the sample (resolution is 50 pm) and then renormalized by dividing it by the experimental transmission T [Fig. 4(c)], then suitably smoothed, and finally divided by A (which is proportional to the input power), namely, $S = S_{\mathrm{OSA}}/T/A$.

3. Analytic PSA theory

A general form for the PSA equation is given in Refs. [13,23]. We summarize the theory here. In the one-mode PSA, the two signal input fields are identical, namely, $A_1 = A_2 = A\exp(i\Delta\varphi/2)$, the phase being relative to the pump. The gain is then

$$g(\Delta\varphi) = \cosh(\kappa L)^2 + 2\frac{\delta\overline{\gamma}}{\kappa^2}\sinh(\kappa L)^2\cos(\Delta\varphi) - 2\frac{\overline{\gamma}}{\kappa}\sinh(\kappa L)\cosh(\kappa L)\sin(\Delta\varphi). \quad \text{(A1)}$$

Here, $\kappa^2 = |\overline{\gamma}|^2 - \delta^2$, $2\delta = \beta_1 + \beta_2 - \beta_3 - \beta_4 + \gamma(P_3 + P_4)$, and $\overline{\gamma} = 2\gamma A_3 A_4$, being 3 and 4 the two pumps (with $P_j = |A_j|^2$) and γ the nonlinear coupling coefficient. Note that $|\overline{\gamma}|L_{\mathrm{eff}} = \varphi_{\mathrm{NL}}$, which coincides with κL_{eff} at phase matching. In the the pump-degenerate case, $\overline{\gamma} = \gamma P_{\mathrm{pump}}$ and $2\delta = \Delta\beta + 2\gamma P_{\mathrm{pump}}$.

4. Generalized nonlinear Schrödinger equation in PhC waveguides

The propagation of nonlinear pulses in nontranslation-invariant waveguides such as PhCs is possible in the context of the the slowly varying envelope approximation (SVEA), which leads to a nonlinear Schrödinger equation (NLSE) [40]. The field $\mathbf{E}(\mathbf{r},t) = A(z,t)\mathbf{e}(\mathbf{r})\exp[i(kz - \omega t)]$ is represented as a complex envelope modulating the carrier frequency ω and spatial dependence described by the Bloch normal mode $\mathbf{e},\mathbf{h}$, normalized as

$$\int_S d^2r\, \hat{z}\cdot(\mathbf{e}^*\times\mathbf{h} + \mathbf{e}\times\mathbf{h}^*) = 4 \quad \text{(A2)}$$

the integral carried over a surface S perpendicular to the direction of the propagation $\hat{z}$. Consequently, the square module of the field amplitude A equals the instantaneous power in the mode: $|A(z,t)|^2 = P(z,t)$.

We use the generalized NLSE, which contains the *all-orders* Taylor expansion [41] of the waveguide dispersion $k(\omega)$. Since the transform $t \to t - z/v_g$ is used, the expansion starts from the order two, with $k^{(n)} = \partial_\omega k$:

$$\partial_z A = -i\sum_{n=2}^{N}\frac{k^{(n)}}{n!}\partial_t^n A - \frac{\alpha}{2}A + i\gamma(1 + i\tau_s\partial_t)|A|^2 A + L_N^{(3)}. \quad \text{(A3)}$$

The nonlinear response is described by a nonlinear parameter γ and the self-steepening coefficient $\tau_s = \partial_\omega \gamma/\gamma$ (Ref. [41]). The linear attenuation coefficient is α.

This equation describes the nonlinear propagation of pulses, including also parametric frequency mixing (FWM), provided that the interacting waves occupy a spectral band narrow enough to allow the SVEA approximation. In order to account for higher-order nonlinear effects (multiphoton absorption and free-carrier-induced dispersion and absorption), specific terms are added, namely,

$$L_N^{(3)} = ik_0\sigma_n NA + \beta_{3PA}|A|^4. \tag{A4}$$

The first term accounts for free-carrier dispersion and absorption, corresponding to the real and imaginary parts of the coefficient k_0, through the density of free carriers N, which is calculated using an auxiliary rate equation. The second term accounts for three-photon absorption. The nonlinear equation is solved using the Fourier-based split-step method [7]. Each time step is solved in two parts. First, the linear part of the equation is Fourier (anti)transformed [since in our notation $\mathbf{E} \propto \exp(-i\omega t)$], multiplied by a prefactor relating to dispersion and attenuation and then transformed back:

$$\partial_z A\Delta z|_{\text{linear}} = F\{[-i\Delta k(\omega) - \alpha(\omega)]F^{-1}A\}.$$

Here, the prefactor $\Delta k = \sum_{n=2}^{N} \frac{k^{(n)}}{n!} = k(\omega) - (\omega_0) - k^{(1)}(\omega_0)(\omega - \omega_0)$ and $\alpha(\omega)$ express the dispersion of the linear attenuation. The nonlinear part is solved as

$$\partial_z A\Delta z|_{\text{NL}} = i\gamma|A|^2A - i\gamma\tau_s F\{(\omega - \omega_0)F^{-1}(|A|^2A)\}.$$

5. Modeling the PSA using the GNLSE

The all-order approximation allows to account for the exact dispersion $[\Delta k(\omega)]$, as reported in Fig. 4 and the linear losses, which are a smooth function of the group index (this amounts to 30 dB/cm in the operating range), are input in the model. We do not take into account the dips observed in the transmission spectra, at 1550 and 1558 nm.

As initial condition (input) for the calculation, three pulses with a *super*-Gaussian shape $\exp[-(t/t_0)^{2n}]$ are used to match both the measured input spectra and the autocorrelation trace. The Kerr nonlinearity is represented by the nonlinear coupling parameter γ, while the dispersion of the nonlinear response is neglected, although recently it has been shown that it might play a role in the propagation of ultrafast pulses [42].

The nonlinear losses and free-carrier effects are included through the term $L_N^{(3)}$ with parameters taken from Ref. [43]. Importantly, we have compared the calculation with $L_N^{(3)}$ set to zero and concluded that the role of higher-order nonlinearities is negligible, which is consistent with our experiments. The calculation is repeated for each power level (hence φ_{NL}) and value of the relative phase $\Delta\varphi$. The phase-sensitive gain is calculated by following exactly the same procedure described for the experimental data.

6. Calculation of the nonlinear coupling parameter in a PhC waveguide

The nonlinear coupling parameter γ is evaluated for Kerr nonlinearity in isotropic materials [44] using the Lorentz reciprocity theorem applied to the normal modes of the waveguide [45], which yields

$$\gamma_{\text{SPM}} = \frac{\omega n_2 \epsilon_0^2 c_0}{4L} \int_V d^3r\, \epsilon_r \chi_r \frac{2|\mathbf{e}|^4 + |\mathbf{e}\cdot\mathbf{e}|^2}{3}. \tag{A5}$$

The integral is carried out a volume V entailing one period L of the PhC waveguide, $\chi_r = \chi^{(3)}(\mathbf{r})/\chi^{(3)}$, the ratio between the spatial distribution of the nonlinear tensor $\chi^{(3)}(\mathbf{r})$ to a reference value $\chi^{(3)}$ related to the nonlinear index $n_2 = \frac{3\chi^{(3)}}{4\epsilon_0\epsilon_r c_0}$. When the nonlinear material is homogeneous and it is defined within a subvolume V_{NL}, then $\chi_r = 1$ inside it and it vanishes outside.

7. Waveguide design

The complete design entails a waveguide width is $W = 0.95\sqrt{3}a$, while the first row of holes is also displaced outwards by $0.16a$. The radius of the first row is $0.25a$, the second and third is $0.26a$, the radius of the other holes is $0.23a$.

[1] A. E. Willner, S. Khaleghi, M. R. Chitgarha, and O. F. Yilmaz, J. Lightwave Technol. **32**, 660 (2014).

[2] P. P. Absil, J. V. Hryniewicz, B. E. Little, P. S. Cho, R. A. Wilson, L. G. Joneckis, and P.-T. Ho, Opt. Lett. **25**, 554 (2000).

[3] M. A. Foster, A. C. Turner, J. E. Sharping, B. S. Schmidt, M. Lipson, and A. L. Gaeta, Nature (London) **441**, 960 (2006).

[4] L. K. Oxenlowe, Hua Ji, M. Galili, Minhao Pu, Hao Hu, H. C. H. Mulvad, K. Yvind, J. M. Hvam, A. T. Clausen, and P. Jeppesen, IEEE J. Sel. Top. Quantum Electron. **18**, 996 (2012).

[5] J. Li, T. P. White, L. O'Faolain, A. Gomez-Iglesias, and T. F. Krauss, Opt. Express **16**, 6227 (2008).

[6] C. Monat, B. Corcoran, M. Ebnali-Heidari, C. Grillet, B. J. Eggleton, T. P. White, L. O'Faolain, and T. F. Krauss, Opt. Express **17**, 2944 (2009).

[7] G. P. Agrawal, *Nonlinear Fiber Optics*, 3rd ed. (Academic Press, San Diego, 2001).

[8] E. Shumakher, A. Willinger, R. Blit, D. Dahan, and G. Eisenstein, Opt. Express **14**, 8540 (2006).

[9] A. Willinger, S. Roy, M. Santagiustina, S. Combri, A. De Rossi, and G. Eisenstein, Opt. Express **23**, 17751 (2015).

[10] C. M. Caves, Phys. Rev. D **26**, 1817 (1982).

[11] Y. Mu and C. M. Savage, J. Opt. Soc. Am. B **9**, 65 (1992).

[12] H. P. Yuen, Opt. Lett. **17**, 73 (1992).

[13] Z. Tong and S. Radic, Adv. Optics Photon. **5**, 318 (2013).

[14] C. J. McKinstrie, S. Radic, M. G. Raymer, and L. Schenato, Opt. Express **15**, 2178 (2007).

[15] M. Gao, T. Inoue, T. Kurosu, and S. Namiki, Opt. Lett. **37**, 1439 (2012).

[16] D. Levandovsky, M. Vasilyev, and P. Kumar, Opt. Lett. **24**, 984 (1999).

[17] K. Croussore and G. Li, IEEE J. Sel. Top. Quantum Electron. **14**, 648 (2008).

[18] M. E. Marhic, P. A. Andrekson, P. Petropoulos, S. Radic, C. Peucheret, and M. Jazayerifar, Laser Photon. Rev. **9**, 50 (2015).

[19] R. Slavk, F. Parmigiani, J. Kakande, C. Lundstrm, M. Sjdin, P. A. Andrekson, R. Weerasuriya, S. Sygletos, A. D. Ellis, L. Grner-

Nielsen, D. Jakobsen, S. Herstrm, R. Phelan, J. O'Gorman, A. Bogris, D. Syvridis, S. Dasgupta, P. Petropoulos, and D. J. Richardson, Nat. Photon. **4**, 690 (2010).
[20] U. B. Hoff, G. I. Harris, L. S. Madsen, H. Kerdoncuff, M. Lassen, B. M. Nielsen, W. P. Bowen, and U. L. Andersen, Opt. Lett. **38**, 1413 (2013).
[21] Y. Zhang, C. Husko, J. Schr, S. Lefrancois, I. H. Rey, T. F. Krauss, and B. J. Eggleton, Opt. Lett. **39**, 363 (2014).
[22] Y. Zhang, C. Husko, J. Schrder, and B. J. Eggleton, Opt. Lett. **39**, 5329 (2014).
[23] C. McKinstrie and S. Radic, Opt. Express **12**, 4973 (2004).
[24] P. Colman, S. Combrié, G. Lehoucq, and A. De Rossi, Opt. Express **20**, 13108 (2012).
[25] C. Caër, S. Combrié, X. Le Roux, E. Cassan, and A. De Rossi, Appl. Phys. Lett. **105**, 121111 (2014).
[26] Q. V. Tran, S. Combrié, P. Colman, and A. de Rossi, Appl. Phys. Lett. **95**, 061105 (2009).
[27] C. Grillet, L. Carletti, C. Monat, P. Grosse, B. B. Bakir, S. Menezo, J. M. Fedeli, and D. J. Moss, Opt. Express **20**, 22609 (2012).
[28] P. Apiratikul, J. J. Wathen, G. A. Porkolab, B. Wang, L. He, T. E. Murphy, and C. J. K. Richardson, Opt. Express **22**, 26814 (2014).
[29] M. Pu, H. Hu, L. Ottaviano, E. Semenova, D. Vukovic, L. K. Oxenlowe, and K. Yvind, in *Optical Fiber Communication Conference* (Optical Society of America, Washington, DC, 2015), p. Th5A–3.
[30] U. D. Dave, B. Kuyken, F. Leo, S.-P. Gorza, S. Combrie, A. De Rossi, F. Raineri, and G. Roelkens, Opt. Express **23**, 4650 (2015).
[31] R. Neo, J. Schrder, Y. Paquot, D.-Y. Choi, S. Madden, B. Luther-Davies, and B. J. Eggleton, Opt. Express **21**, 7926 (2013).
[32] I. Cestier, S. Combrié, S. Xavier, G. Lehoucq, A. de Rossi, and G. Eisenstein, Opt. Lett. **37**, 3996 (2012).
[33] Y. Zhang, J. Schrder, C. Husko, S. Lefrancois, D.-Y. Choi, S. Madden, B. Luther-Davies, and B. J. Eggleton, J. Opt. Soc. Am. B **31**, 780 (2014).
[34] F. Da Ros, D. Vukovic, A. Gajda, K. Dalgaard, L. Zimmermann, B. Tillack, M. Galili, K. Petermann, and C. Peucheret, Opt. Express **22**, 5029 (2014).
[35] P. Colman, Phys. Rev. A **92**, 013827 (2015).
[36] W. Xie, I. Fsaifes, T. Labidi, and F. Bretenaker, Opt. Express **23**, 31896 (2015).
[37] L. H. Frandsen, A. V. Lavrinenko, J. Fage-Pedersen, and P. I. Borel, Opt. Express **14**, 9444 (2006).
[38] J. Kakande, R. Slavk, F. Parmigiani, A. Bogris, D. Syvridis, L. Grner-Nielsen, R. Phelan, P. Petropoulos, and D. J. Richardson, Nat. Photon. **5**, 748 (2011).
[39] F. Parmigiani, G. D. Hesketh, R. Slavik, P. Horak, P. Petropoulos, and D. J. Richardson, IEEE Photon. Technol. Lett. **26**, 2146 (2014).
[40] N. A. R. Bhat and J. E. Sipe, Phys. Rev. E **64**, 056604 (2001).
[41] T. Brabec and F. Krausz, Phys. Rev. Lett. **78**, 3282 (1997).
[42] C. Husko and P. Colman, Phys. Rev. A **92**, 013816 (2015).
[43] C. Husko, S. Combrié, Q. Tran, F. Raineri, C. Wong, and A. De Rossi, Opt. Express **17**, 22442 (2009).
[44] R. W. Boyd, *Nonlinear Optics*, 2nd ed. (Elsevier, Amsterdam, 2003).
[45] D. Michaelis, U. Peschel, C. Wächter, and A. Bräuer, Phys. Rev. E **68**, 065601 (2003).